CHAPTER 114

OFFSHORE TSUNAMI PROFILES OBSERVED AT THE COASTAL WAVE STATIONS

Toshihiko NAGAI[1], Noriaki HASHIMOTO[2],
Kazuyoshi SHIMIZU[3], and Fujio KITAMURA[4]

ABSTRACT

This paper presents offshore tsunami profiles observed by NOWPHAS (Nationwide Ocean Wave Information Network for Ports and Harbours) wave-measuring instruments installed at various coastal wave stations and tide stations in Japan. Included are wave profiles of damage-inflicting tsunamis generated by the 1993 Hokkaido-Southwest Earthquake, the 1994 Hokkaido-Eastoff Earthquake, the 1996 Iri-Anjaya Earthquake, and other smaller recently occurring tsumamis. Also presented are characteristiscs and phenomena of interest clarifed through various analyses performed on observational data.

Introduction

Analysis of observed offshore tsunami profiles provides valuable information for clarifying their charactertics, which is essential for preventing disasterous consequences. Here, we present profiles of several damage-inflicting tsunamis which recently struck Japan, i.e., tsunamis generated by the 1993 Hokkaido-Southwest Earthquake on Jul.12, 1993, the 1994 Hokkaido-Eastoff Earthquake on Oct.4, 1994, the 1995 Hyogo-South Earthquake on Jan.17, 1995, and the 1996 Irianjaya Earthquake on Feb.17, 1996. Wave data was measured by NOWPHAS (Nationwide Ocean Wave Information Network for Ports and Harbours) wave-measuring instruments installed at various coastal wave stations and tide stations in Japan. Also presented are characteristics and phenomena of interest clarifed through various analyses performed on observational data.

---

[1] Chief, Marine Observation Laboratory, Hydraulic Engineering Divison, Port and Harbour Research Institute (PHRI), Ministry of Transport (MOT), 3-1-1 Nagase, Yokosuka, 239, Japan
[2] Chief, Hydraulic Laboratory, Marine Environmental Divison, PHRI, MOT
[3] Ex-Senior Research Engineer, Hydraulic Engineering Divison, PHRI, MOT
[4] Ex-Senior Research Engineer, Coastal Development Institute of Technology, 6F 3-16 Hayabusa-cho, Chiyoda, Tokyo, 102, Japan

Wave-Measuring Instrumentation

Figure 1 shows the NOWPHAS wave observation network in Japan (Nagai et al., 1996, 1994a) which is operated under the conspices of the Ports and Harbours Bureau of the Ministry of Transport (MOT) and its associated agencies including the Port and Harbour Research Institute (PHRI). This nationwide network of wave-measuring instrumentaion is the product of long-term intensive efforts directed at obtaining more precise and reliable coastal wave information for disaster prevention purposes and the planning, design, and construction of ports and other coastal structures.

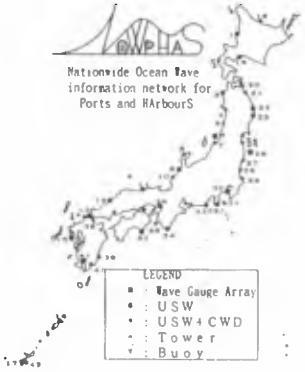

Figure. 1 NOWPHAS Wave Observation Network

Figure 2 shows three types of wave-measuring instruments employed in the NOWPHAS network: (1) The ultrasonic wave (USW) gauge, a widely employed instrument (jointly developed by the Kaijo Co. and PHRI in the 1960s) which precisely determines wave surface elevation by measuring the time for an ultrasonic wave to travel between the seabed and water surface, (2) The current wave directional (CWD) gauge, a widely employed instrument (developed in the 1970s) which determines wave direction by measuring wave-induced horizontal current fluctuations along the seabed, and (3) The Doppler wave directional meter (DWDM), a newly employed instrument (jointly developed by the Kaijo Co., Marine Surveyors Associa-tion, and PHRI in 1995) which uses a single sensor to determine with sufficient accuracy the height, period, and directional spectra of waves. DWDMs have been installed at four coastal stations (Fig. 1) (Takayama etal., 1995), and in the future are expected to be the main wave-measuring instrument employed under NOWPHAS.

Figure. 2 USW, CWD, and DWDM Wave Gauges

Hokkaido-Southwest Earthquake OffshoreTsunami Profile

Figure 3 shows 20 min of offshore wave records observed at coastal station No.8 Wajima (Sta.8) before arrival of the 1993 Hokkaido-Southwest Earthquake tsunami. Shown are water surface elevation, horizontal current at the seabed in vector form, and the corresponding vector components of water velocity U(m/s) and water direction θ. A USW installed at 50 m measures η and a CWD installed at 27 m measures U and θ. Figure 4 shows corresponding records observed just after the arrival of the tsunami (Nagai etal.,1993,1994b,1995a), where it can be seen from the center line determined by low-pass filtering that distinct, long-period oscillations are generated in η. The wave current is also clearly affected as indicated by the long-period oscillations in the horizontal current vectors numerically determined using a triangular low-pass filter of 10s in length.

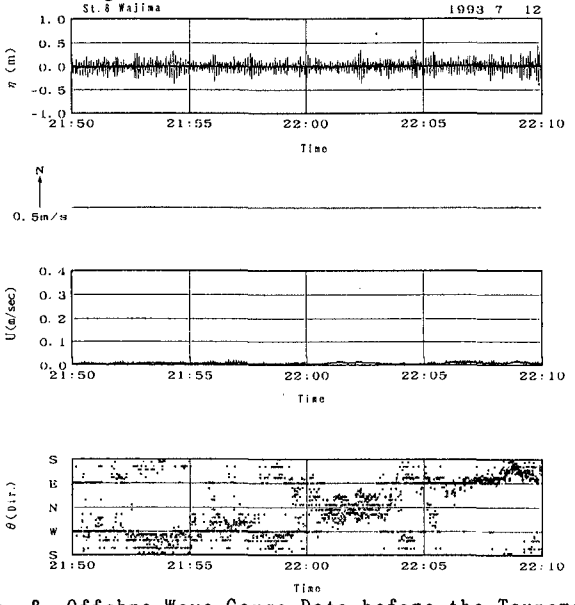

Figure. 3 Offshre Wave Gauge Data before the Tsunami Attack

Shown in Figure 5 are pair values of USW-measured filtered η and CWD-measured differential change in seabed pressure p observed at Sta.4 Akita before (left) and after (right) tsunaimi arrival; where for each case, 20 min of data are plotted at a sampling interval of 0.5s. Before arrival, most values are concentrated around the origin (η=p= 0) indicating no long-period oscillations in η or seabed current. In contrast, however, after the tsunami arrives they are concentrated along the line η=p; thereby indicating long-period oscillations occur as expected under linear long wave theory. Taken together, these results confirm the reliability of the observed.

Under linear progressive long wave theory, the following relationship should hold:

$$U_{max} = (\eta / 2)(g/h)^{-1/2} \quad (1)$$

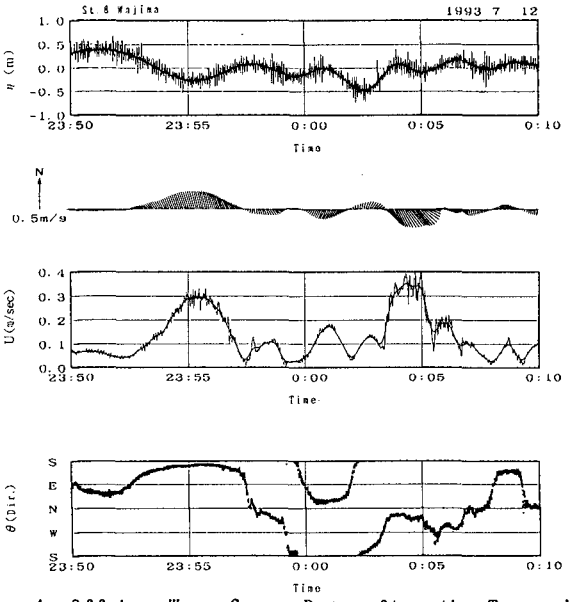

Figure. 4 Offshre Wave Gauge Data after the Tsunami Attack

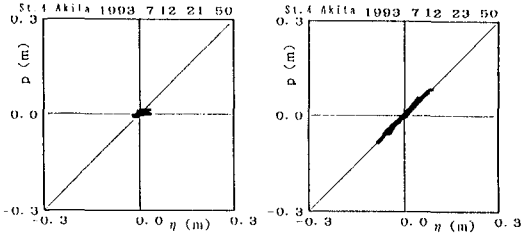

Figure. 5 Comparison of η and p

where U_{max} is the maximum horizontal water velocity at the seabed, $\eta/2$ the amplitude of water surface elevation $(\eta_{max} - \eta_{min})/2$, g the acceleration of gravity, and h the water depth. These parameters are respectively plotted as pair values in Figure 6 for various wave stations over a 20-min period following the arrival of the tsunami. If eq. (1) is satisfied, then the plotted values should fall on the indicated 45 degree line. For standing waves, $\eta=0$ at the nodes (y-axis) and U=0 at the antinodes (x-axis). Considering the results, it appears that the observed tsunami is not completely progressive, but rather exhibits characteristics of standing waves due to the effect of wave reflection.

Integration of current velocity over time gives the motion of water particles at the seabed, being shown in Figure 7 for 20 min before and after the tsunami's arrival at Sta. 8 with and without tide corrections. Motion is shown in the horizontal plane in which the x- and y-axis indicate directions East(+) and West(-) and North(+) and South(-). The effect of the tsunami is quite apparent, especially when considering tide effects. Note that the direction of the constant-velocity tidal current is shown before arrival, and that after correction it is

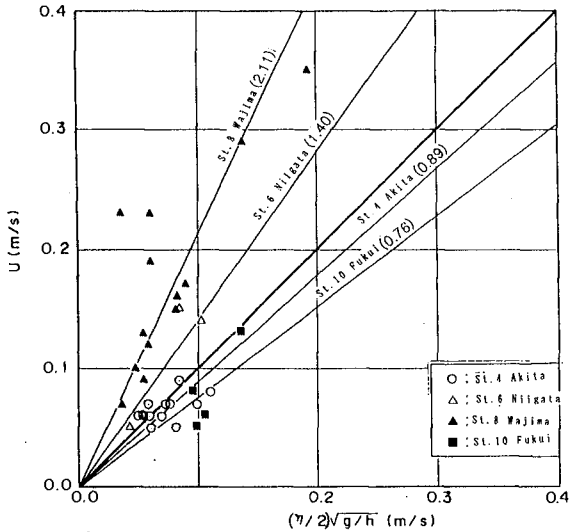

Figure. 6 Comparison of η and U

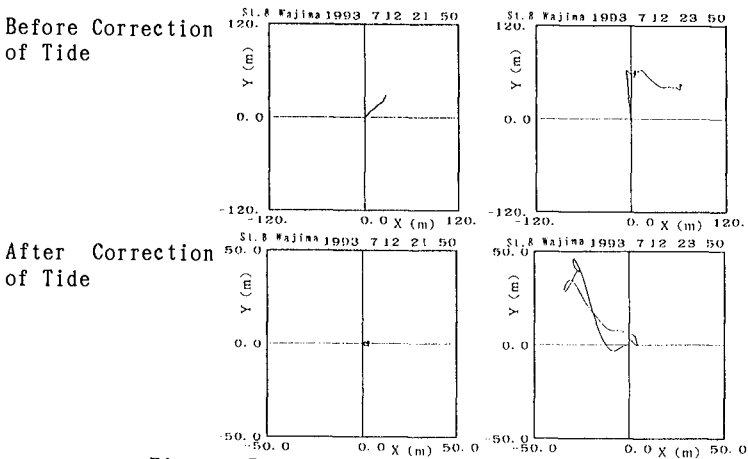

Figure. 7 Seabed Water Particle Movement

properly accounted for. The amplitude of seabed particle motion due to the tsunami is shown to be about 50m, i.e., a distance much greater than can be explained by even the strongest wind-wave conditions.

Figure 8 shows the low-pass filtered offshore wave profile η and tide record Z, before and until more than 6 hours after tsunami arrival as measured at Sta.8 (3km offshore), and the Wajima Port tide station, respectively. Upon tsunami arrival just after 0:00LT, both records show a large peak which cannot be accounted for by the effects of wind or tidal motions. In addition, short-period oscillations less than 10 min, i.e., such as those clearly shown in η, cannot be observed in tide records due to the occurrence of low-pass-filter effects in the measuring instrument's seawater drain tube; thereby demonstrating the

necessity for deploying offshore wave-measuring instrumentation.

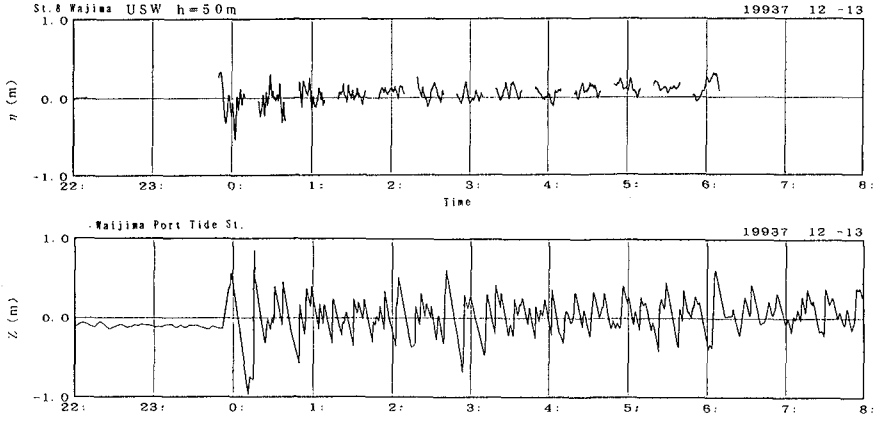

Figure. 8 Comparison of Offshore Wave Profile and Tide Record

Hokkaido-Eastoff Earthquake Offshore Tsunami Profile

Figure 9 summarizes the heights and periods of the tsunami generated by the 1994 Hokkaido-Eastoff Earthquake as observed along Japan's Pacific Ocean coast by NOWPHAS wave-measuring instrumentation (Nagai et al., 1995b, 1995c). Individual tsunami waves was defined by the zero-up-cross method. A "*" denotes wave station data while all other data is from tide stations. Note that individual tsunami waves show a long period of about 40 min.

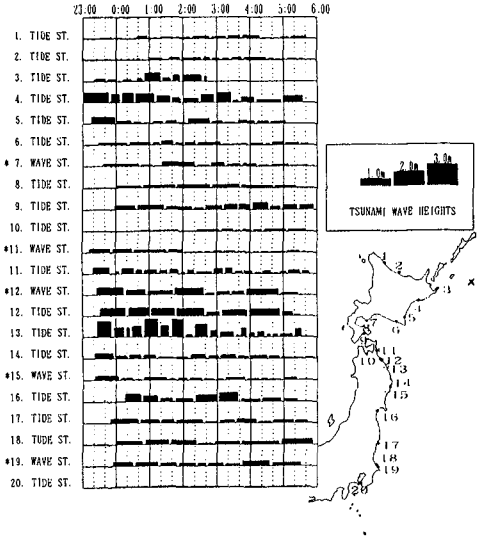

Figure. 9 Tsunami Heights and Periods of the 1994.10 Earthquake

Figure 10 shows a continuous offshore profile η of the tsunami as observed at Sta. 19 off Tomakomai Port at a water depth of 18.5 m. This data was obtained as part of a continuous offshore long wave observation project conducted in Oct. 1994 by the Tomakomai Port Construction Office of the Hokkaido Development Agency in order to investigate a port resonance problem caused by long waves. Although η is low-pass filtered, clearly distinguishing the tsunami from wind waves and tides is difficult due to the presence of waves with significant wave heights of more than 2 m and a large range of tidal motion. Nevertheless, when these observations are considered in conjunction with those in Figure 10, this confirms the presence of tsunami-generated waves with very long periods of 30 to 80 min.

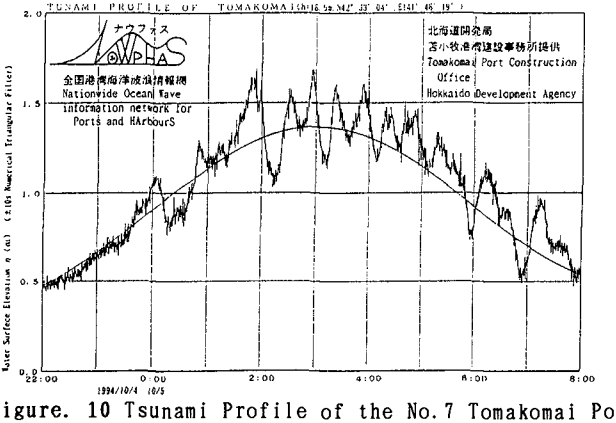

Figure. 10 Tsunami Profile of the No. 7 Tomakomai Port

Figure 11 also shows continuous tsunami wave data observed by tide and offshore wave stations at Sta. 20 Mutsu-Ogawara for the tsunamis generated by the Hokkaido-Eastoff and 1994 Sanriku-Faroff (Dec. 28, 1994) Earthquakes. Also shown are the predicted tides, as well as seabed horizontal current vectors for the Hokkaido-Eastoff tsunami.

The results of applying frequential spectral analysis to the data in Figure 11 are presented in Figure 12, which shows corresponding power spectra and the response functions of the wave and tide gauges for each tsunami. Note that both tsunami show the same correlation between their wave and tide spectra; thereby indicating accurate and reliable measurements even under transient, unstable conditions caused by a tsunami.

Figure 13 shows the results of a spectral correlation analysis between η and Z power spectra determined from observation data of the Hokkaido-Eastoff tsunami. Coherence and phase values indicate high stability for measurements at frequencies less than 10^{-3}Hz, which includes the frequency range where dominant tsunami energy exists.

Shown in Figure 14 are corresponding results for spectral correlation analysis between η and the two vector components of seabed horizontal current velocity u and v, where u is the east-west (on-off shore) direction and v the north-south (longshore) direction.

Evaluation of the respective coherence and phase values indicates consistent results with those shown in Figure 13.

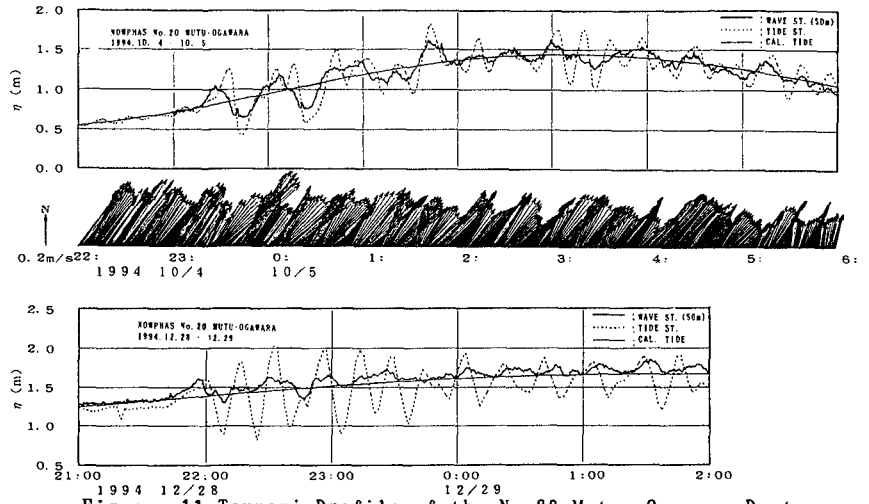

Figure. 11 Tsunami Profile of the No. 20 Mutsu-Ogawara Port

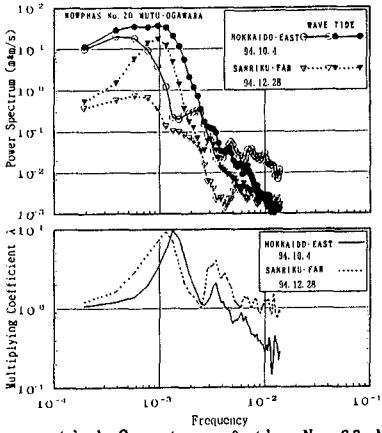

Figure. 12 Frequential Spectra of the No. 20 Mutsu-Ogawara Port

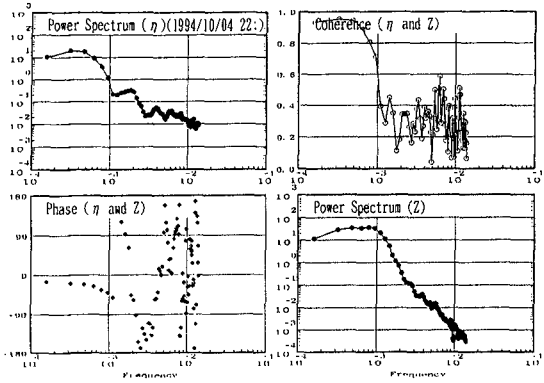

Figure. 13 Spectra Correlation between η and Z

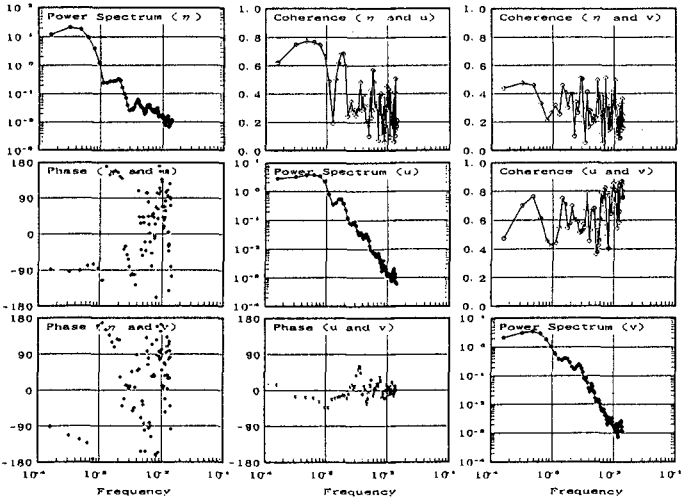

Figure. 14 Spectra Correlation among η, u and v

Figure 15 shows pair values of u and $\eta\,(g/h)^{-1/2}$ plotted over three 15-min periods in which the first-arriving individual Hokkaido-Eastoff tsunami wave was observed by Sta. 20, where the values should fall on the straight line passing through the origin under linear progressive wave theory. In this case, the difference between the observation depth of the USW (50m) and CWD (28m) gauges is accounted for. A comparison of observed values indicates the presence of standing wave characteristics at the early stage of observation due to wave reflections off the coast.

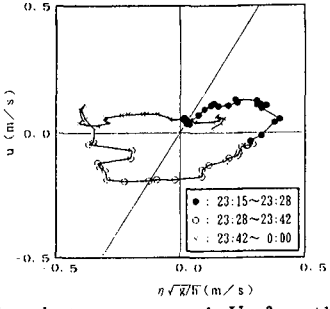

Figure. 15 Relation between η and U for the First Tsunami Wave

Continuous-observed offshore wave profiles provide a good benchmark from which to evaluate numerical models for simulating tsunami characteristics. Figure 16 compares observed wave/tide station η/Z and u of the Hokkaido-Eastoff tsunami obtained at Sta. 20 with those calculated by a numerical simulation model of 3 km grid based on linear long wave propagation characteristics(Aida, 1962), and the initial seabed movement determined by the DCRC-3b model (Table 1) developed at the University of Tohoku. Good agreement is present for all three measured parameters, possibly being due to employing a grid size that is relative

-ly small compared to tsunami wave length with a 40-min period.

Table. 1 The 1994 Tsunami Model (DCRC-3b Model by Univ. of Tohoku)

Origin of Fault	$43.210°N, 146.120°E$
Length	$140km$
Wideth	$70km$
Strike	52°
Dip Angle	77°
Slip Angle	128°
Depth	$30km$
Dislocation	$7.62m$

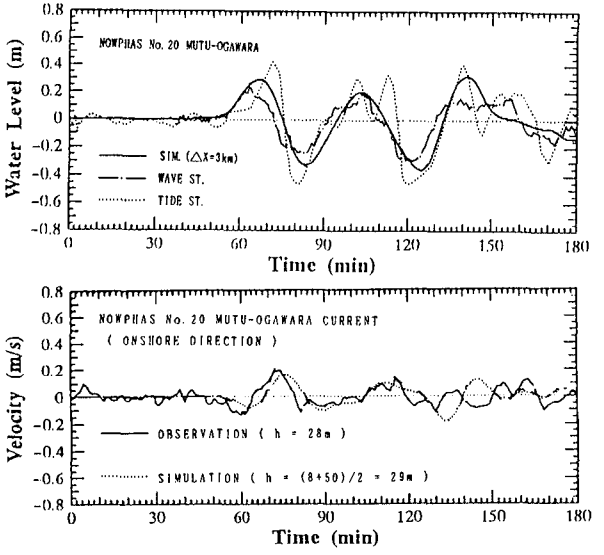

Figure. 16 Comparizon of the Observed and Calculated Tsunami Profile

Hyogo-South Earthquake Tsunami Profile

The city of Kobe and its surrounding region suffered tremendous damage and loss of life when the 1995 Hyogo-South Earthquake stuck during the early morning hours (05:47). Figure 17 shows USW-measured off-shore wave profile before and immediately after striking as observed by Sta.36 Kobe, where amplitudes of several centimeters and periods of 1 or 2 min are indicated by the low-pass-filtered line, i.e., most of the earthquake's energy was expended on land areas such that its effect generated only slight movement of the seabed.

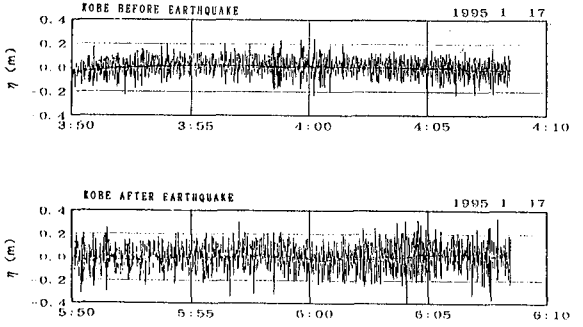

Figure. 17 The 1995 Hygo-South-Earthquake Tsunami Profile

Irianjaya Earthquake Tsunami Profile

Figure 18 shows the wave profile of the tsunami generated by the 1996 Irianjaya-Earthquake as observed by Sta. 31 Habu (USW, 50 m) and PHRI (USW and tide station) at the entrance to Tokyo Bay 50 km distant. The tsunami arrived at the bay entrance 20 to 30 min after initial observation at Sta. 31, which indicates that continuous observation and monitoring of offshore waves at this offshore station would allow predicting the strike time and provide an early warning for the Tokyo area. Note that the maximum wave heights are about 10 and 70 cm, respectively, with this amplification in height being due to topographical resonance effects.

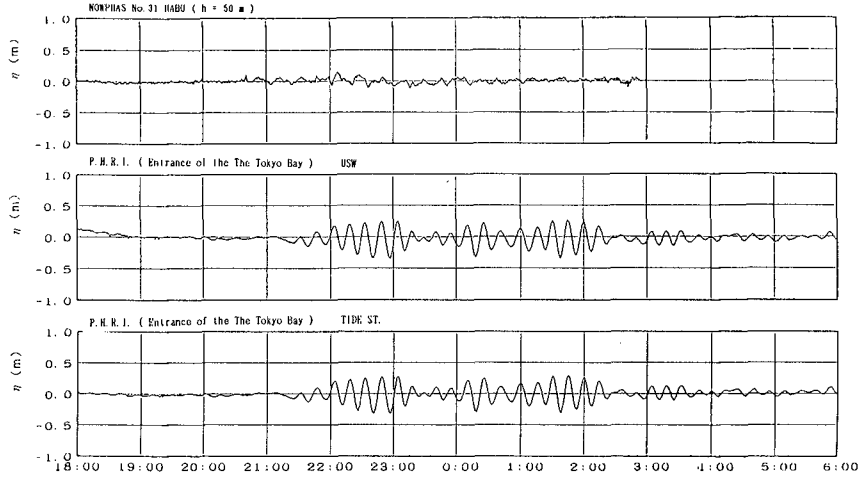

Figure. 18 The 1996 Irianjaya-Earthquake Tsunami Profile

The results of applying frequential spectral analysis to the data in Figure 18 are presented in Figure 19, where a distinct resonance peak is apparent and indicates that amplification occurs in the frequency band of $0.9*10^{-3}$ and $1.5*10^{-3}$Hz (T = 18.5 and 11 min).

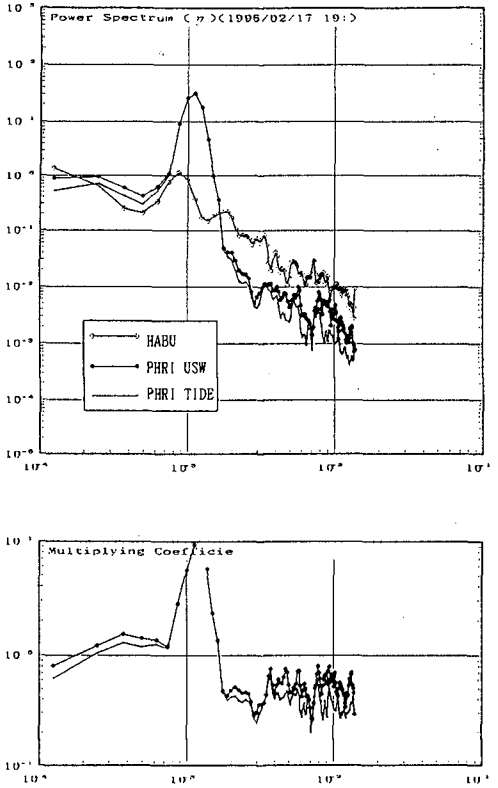

Figure. 19 Frequential Spectra of the 1996 Irianjaya-Earthquake Tsunami

Summary

We have analyzed selected wave profiles and associated data of large, recently striking tsunami as observed by NOWPHAS offshore wave-measuring instruments and harbor tide stations throughout Japan. As a result of our analysis, several tsunami characteristics and phenomena of interest have been clarified, and through our better understand we can expect to improve observation capability. To fully understand the characteristics of tsunamis and long waves, however, the data acquisition system of NOWPHAS must be reconfigured to a more continuous observa-tion scheme as wave observations are at the present time only performed for 20min every 2h. Efforts to realize such an observation system are now in progress (Nagai etal.,1995d).

Acknowledgments

For their outstanding cooperation, sincere gratitude is extended to all personnel involved with NOWPHAS, with a special thank you to those from the Ports and Harbours Bureau, District Port Construction Bureaus of MOT, Hokkaido and Okinawa Development Agencies, and PHRI.

REFERECES

Aida, I. (1962), "Numerical Experiments for Tsunami Caused by Moving Deformation of the Sea Bottom, Bull. Earthqu. Res. Inst., vol. 47, pp. 849-862

Nagai, T., Sugahara, K, Hashimoto, N., and Asai, T. (1996), "Annual Report on Nationwide Ocean Wave information network for Ports and HArbourS (NOWPHAS 1994)", Technical Note of the PHRI, No. 821, 313p.
from 1970 to 1993 year's versions of the same series of the Annual Reports, See the Technical Notes of the PHRI, No. 137, 158, 178, 209, 233, 258, 282, 311, 332, 373, 417, 445, 480, 517, 545, 574, 612, 642, 666, 712, 721, 745, 770, and 796 respectively

NAGAI, T., HASHIMOTO, N., SHIMIZU, K., and TAKAYAMA, T. (1995a), "Tsunami Profiles Observed at the NOWPHAS Offshore Wave Stations", Second International Workshop on Wind and Earthquake for Offshore and Coastal Structure, UJNR at Berkeley, California

Nagai, T., Hashimoto, N., Hiraishi, T, and Shimzu K. (1995b), "Characteristics of the 1994 Hokkaido-Eastoff-Earthquake Tsunami", Technical Note of the PHRI, No. 802, 97p.

Nagai, T., Hashimoto, N., Hiraishi, T, Shimzu K., Ichikawa, T., Miyabe S., Kudaka, M., and Kawamata, S. (1995c), "Characteristics of the 1994 Hokkaido-Eastoff-Earthquake Tsunami based on the Field Observation Data", Proceedings of Coastal Engineering, Vol. 42, Japan Society of Civil Engineers, pp. 351-355

Nagai, T., Hashimoto, N., Asai, T., Tobiki, I., Ito, K., Toue, T., Kobayashi, A. and Shibata, I. (1995d), "Relationship of a Moored Vessel in a Harbour and a Long Wave Caused by Wave Groups", Proceedings of the 24th International Conference on Coastal Engineering (ICCE'94), vol. 1, pp. 847-860

Nagai, T., Sugahara, K., Hashimoto, N., Asai, T., Higashiyama, S., and Toda, K. (1994a), "Introduction of Japanese NOWPHAS System and its Recent Topics", Proceedings of HYDRO-PORT'94, PHRI, pp. 67-82,

Nagai, T., Sugahara, K, Hashimoto, N., and Asai, T., Higashiyama, S., Toda, K. (1994b), "Offshore Tsunami Profiles of the 1993 Hokkaido-Southwest-Earthquake Tsunami", Proceedings of Coastal Engineering, Vol. 41, Japan Society of Civil Engineers, pp. 221-225,

Nagai, T., Hashimoto, N., and Asai, T. (1993), "The Hokkaido-Southwest-Earthquake Tsunami profiles observed at the NOWPHAS offshore stations", Rept. of PHRI, Vol. 32, No. 4, pp. 51-97

TAKAYAMA, T., HASHIMOTO, N., NAGAI, T., TAKAHASHI, T., SASAKI, H., and ITO, Y., (1995), "Development of Submerged Doppler-type Directional Wave Meter", Proc. of the 24th International Conference on Coastal Engineering (ICCE'94), vol. 1, pp. 624-634